Adaptive neural sliding mode control for heterogeneous ship formation keeping considering uncertain dynamics and disturbances

You, Xu; Yan, Xinping; Liu, Jialun; Li, Shijie; Negenborn, Rudy R.

DOI
10.1016/j.oceaneng.2022.112268

Publication date
2022

Document Version
Final published version

Published in
Ocean Engineering

Ocean Engineering 263 (2022) 112268

Contents lists available at ScienceDirect

Ocean Engineering

journal homepage: www.elsevier.com/locate/oceaneng

Adaptive neural sliding mode control for heterogeneous ship formation keeping considering uncertain dynamics and disturbances☆

Xu You [a,b,c], Xinping Yan [b,c], Jialun Liu [b,c,*], Shijie Li [a], Rudy R. Negenborn [d]

[a] School of Transportation and Logistics Engineering, Wuhan University of Technology, Wuhan, China
[b] Intelligent Transportation Systems Research Center, Wuhan University of Technology, Wuhan, China
[c] National Engineering Research Center for Water Transport Safety, Wuhan University of Technology, Wuhan, China
[d] Department of Maritime and Transport Technology, Delft University of Technology, Delft, The Netherlands

ARTICLE INFO

Keywords:
Heterogeneous formation
Formation control
Adaptive control
Neural networks
Heterogeneous dynamics

ABSTRACT

This paper investigates the formation keeping problem of heterogeneous ships with underactuated inputs, uncertain dynamics, and environmental disturbances. The control objective is to make the heterogeneous followers keep the desired formation while tracking a leader. To solve the problem effectively, a novel virtual leader–follower formation scheme considering the ship heterogeneity is proposed by utilizing the backstepping method, adaptive neural network, and adaptive control law. The stability of the formation control system is proved based on Lyapunov's direct method where all tracking errors are guaranteed to be uniformly ultimately bounded. Finally, simulations and comparisons are conducted to verify the effectiveness of the proposed control law.

1. Introduction

1.1. Motivation

In recent years, the formation control of multiple autonomous marine surface vessels has attracted huge attention due to its advantages in widespread applications in water space (Zereik et al., 2018). By selecting appropriate control strategies, formation controller can ensure a group of ships keeps the desired relative posture, maintains the coordinated movement, and finally completes a specific task (Ren and Cao, 2011; Chen and Wang, 2005). Compared to individual applications, formation applications can improve the efficiency of repetitive or continuous tasks. Relevant applications can be roughly summarized from military to civil missions, such as unmanned patrolling, surveillance, unmanned convoying, marine survey, environment monitoring, rescue, and cargo delivering. The existing applications and research mainly prefer to use small unmanned surface vessels (USVs) to carry out theoretical verification due to their good control performance and accessibility. Nevertheless, huge demands on the economy and carbon emissions attract research on large ships, especially on cargo delivery ships.

In 2017, to solve the problem of cargo transportation in the inland river and short sea, Novimar (2017) has put forward the concept of Vessel Train and done some research on ship design, logistics transportation strategy, formation controller design, and so on (Munim, 2019; Haseltalab et al., 2019; Chen et al., 2019). Virtual simulation experiments of Vessel Train are carried out in MARIN to test the proposed formation controller. Moreover, full-scale demonstrations are executed to show their effectiveness on real ships. Additionally, this project has put forward a lot of effective suggestions from logistics, control, policy, emissions, and other aspects (Colling and Hekkenberg, 2019; Colling et al., 2021; Meersman et al., 2020a,b). However, the NOVIMAR project aims at exploring the accessibility of isomorphic formation control considering the existing European navigation environment and the current technological development, where heterogeneous ships are considered a huge challenge and are neglected because of the technical difficulties among different ships. Thus, formation control of heterogeneous ships is changeable and is worthy of study.

A vessel can be taken as an agent in development of the formation control algorithm. Isomorphic agents are widely considered in formation control on robots, planes, vehicles, and ships, where the research objects are defined with the same maneuverability and types. Specifically on previous research, isomorphic agents are regarded to have the same dynamic model and even the same parameters. However, the research objects in real world are not the same. It is of great

☆ Supported by the National Natural Science Foundation of China (62003250), and Southern Marine Science and Engineering Guangdong Laboratory (Zhuhai) (SML2021SP101).

* Corresponding author at: Intelligent Transportation Systems Research Center, Wuhan University of Technology, Wuhan, China.
E-mail address: jialunliu@whut.edu.cn (J. Liu).

https://doi.org/10.1016/j.oceaneng.2022.112268
Received 16 March 2022; Received in revised form 8 August 2022; Accepted 9 August 2022
Available online 21 September 2022

challenge to figure out the performance of heterogeneous controlled objects. In previous studies, heterogeneous agents can be summarized into two aspects. One is the different dynamic model, usually, the control objects are divided into first-order, second-order, or high-order multi-agent systems (Zheng et al., 2011; Shimin et al., 2020), for example, the formation between unmanned aerial vehicles (UAVs) and unmanned ground vehicles (UGVs) (Rahimi et al., 2014). The other aspect is the different heterogeneity dynamics in the same dynamic model, where, for example, (Liu et al., 2021) stresses the heterogeneity dynamics in AUVs. Similar to these heterogeneous agents, heterogeneous ships are assumed to equip with different maneuverability and control characteristics. The heterogeneous features may come from different ship types, ship parameters, propulsion systems, and those properties that have effects on control performance. Some studies have noticed the heterogeneity of hydrodynamics caused by currents and waves (Yuan et al., 2017). However, these studies do not consider other heterogeneous characteristics. Compared with isomorphic ship formation, research on heterogeneous ship formation need to focus on the more important issue: universality of formations. From the perspective of control, the factors on heterogeneous formation can be concluded as follows:

1. The static differences of ships including ship coefficients, scale, propulsion, and other fixed features that will not change during the navigation;
2. The dynamic differences of ships including ship draft, load, speed, and other changeable motion parameters;
3. The disturbances differences including internal ship motion model uncertainties, external environment disturbances, communication errors, control delay, system response time, and other unknown factors.

Motivated by previous research, this study concerns how to apply formation control technology to heterogeneous ships with different maneuverability and types. In this study, the differences are described by using different ship parameters considering the same ship motion model. Ship unknown dynamics and uncertain disturbances are both considered during the formation control process.

1.2. Related works

Usually, the establishment of the formation control algorithm needs to consider the kinematic model of the research object first. Then, the matrix form is used to describe the formation structure and the control methods are determined by choosing different targets and objects. The Lyapunov method is also demonstrated to guarantee the stability of the proposed controller (Oh et al., 2015; Das et al., 2016). Peng et al. (2020) has concluded some core issues on formation control problems, where the preliminary issues could be summarized as non-linearity, uncertainty, under-actuation, constrained variables, unmeasured states, scare communication bandwidth, and collision avoidance. From the classification of formation structure, three common formation modes are summarized including: leader–follower approach (Wang et al., 2020b; Peng et al., 2020), virtual-structure approach (Liu et al., 2017; Gu et al., 2019; Fu et al., 2017), and behavior-based approach (Arrichiello et al., 2006). All these methods have their advantages and shortcomings (Ghommem et al., 2007). Moreover, other approaches like graph theory (Li and Zheng, 2018), and the artificial potential function (Li and Zheng, 2018) are receiving more and more attention due to the systematic research on their information flow and formation structure.

The most common and efficient method is the leader–follower approach. After Breivik et al. (2008) proposed the initial leader–follower formation control scheme on ships by using three degrees of freedom (DOF) on the full actuated ship model. 4 DOFs underactuated ship models are considered in (Chen et al., 2020) to guarantee the formation error limiting in finite time. However, high-order DOFs need more input degrees, which are not common in real ships due to the under-actuation. Thus, 3 DOFs is appropriate to describe the characteristics of the formation control.

Since the sliding mode control (SMC) has been successfully employed in the area of formation control problems owing to its strong robustness and simplicity. Many research have modified SMC algorithms to solve formation problems. Sun et al. (2018) proposed the SMC controller with estimation on ship unknown parameters and the environment disturbances. Wang et al. (2020b) improved the SMC structure with PI sliding surface and introduced the command filter based on the dynamic surface control technique (DSC). Wang et al. (2020a) has simplified the design process of the backing stepping design and reduced the influence of high-frequency measurement noise. The input constraints of formation control on ships are considered in (Riahifard et al., 2020), where neurodynamic optimization and fuzzy approximation are presented as well to solve the uncertainties of disturbances and unknown dynamics. Lu et al. (2018) proposed a novel robust adaptive formation control scheme based on the minimal learning parameter (MLP) algorithm and the disturbance observer (DOB), which reduces the computational effort and increases the ability to compensate the external disturbances. Nevertheless, most researchers have used same ship dynamic models to verify the effectiveness of their proposed formation controller. They lack discussions on the performance of heterogeneous dynamics between different ships.

1.3. Study organization

In this study, we emphasize the ship formation performance with heterogeneous parameters according to the summarized reasons for the heterogeneity features. To solve the problem of controlled objects on under-actuated heterogeneous cargo ships, the static differences of heterogeneity parameters are first considered. Furthermore, the formation control problems are extended from isomorphic ships to heterogeneous ships with the consideration of uncertain dynamics and unknown disturbances.

The main contributions of this work can be summarized as follows:

1. The ship formation controller with heterogeneity ship dynamics, time-varying disturbances, and uncertainties is investigated. Especially, the heterogeneous features of ship control aspects are summarized.
2. The static ship heterogeneity dynamics are considered during the formation controller design, and the results show that the proposed controller has high compatibility and adaptability in both isomorphic and heterogeneous formation keeping problems.
3. Considering the factors on formation control, including the internal errors caused by ship model uncertainty and external errors caused by the environmental disturbances, the proposed controller can achieve effective control performance. To make the formation scheme smoother and less complex, methods of limiting virtual control speed, using offline rolling RBF networks are introduced to improve the computing performance of the control law.

This research is organized as follows: the kinematic and kinetics model of an underactuated ship with heterogeneity dynamics, model uncertainties, and unknown disturbances are introduced in Section 2, where the virtual leader–follower formation structure is demonstrated as well. In Section 3, a preliminary controller with improved virtual speed selection is established for the structure of the formation controller. Furthermore, consideration on ships' uncertain dynamics and external disturbances are well approached by adaptive estimation and approximation approaches in Section 4. Additionally, the stability and robustness are verified by the Lyapunov direct method. Simulation results and analysis on isomorphic and heterogeneous ship models are given out in Section 5. Finally, Section 6 concludes the paper.

2. Problem formulation

2.1. Dynamic model of a ship

As ship control is very complicated due to the complexity of the ship motion model, unknown hydrodynamics estimation, and so on. To simplify this process and ensure the control accuracy, a three DOFs underactuated ship model including surge, sway, and yaw is considered. According to (Fossen, 2011), it can be described as:

$$\begin{cases} \dot{x} = u\cos(\psi) - v\sin(\psi) \\ \dot{y} = u\sin(\psi) + v\cos(\psi) \\ \dot{\psi} = r \\ \dot{u} = \left(\left(m_{22}vr - d_{11}u - f_u\right) + \tau_u + \tau_{wu}\right)/m_{11} \\ \dot{v} = \left(\left(-m_{11}ur - d_{22}v - f_v\right) + \tau_{wv}\right)/m_{22} \\ \dot{r} = \left(\left(m_{11} - m_{22}\right)uv - d_{33}r - f_r + \tau_r + \tau_{wr}\right)/m_{33}, \end{cases} \tag{1}$$

where (x, y, ψ) denote the gravity displacements and heading angle in the earth-fixed frame. (u, v, r) are surge, sway, and yaw velocity, respectively. (m_{11}, m_{22}, m_{33}) denote the ship inertia coefficients including added mass effects. (d_{11}, d_{22}, d_{33}) represent the hydrodynamic damping coefficients. $(\tau_{wu}, \tau_{wv}, \tau_{wr})$ denote the time-varying external environment disturbance including waves, currents, winds, and other disturbances. (f_u, f_v, f_r) are the ship uncertain dynamics. $(\tau_u, 0, \tau_r)$ are the underactuated inputs.

Remark 2.1. Suppose that the external disturbances $(\tau_{wu}, \tau_{wv}, \tau_{wr})$ satisfy

$$\left|\tau_{wu}\right| \le \left|\tau_{wu}^*\right|, \qquad \left|\tau_{wv}\right| \le \left|\tau_{wv}^*\right|, \qquad \left|\tau_{wr}\right| \le \left|\tau_{wr}^*\right|, \tag{2}$$

where the $\tau_{wu}^* > 0, \tau_{wv}^* > 0, \tau_{wr}^* > 0$ present that the upper bounded of external disturbances.

Here are some basic lemmas that can be referred to in the context.

Lemma 1. *According to literature (Polycarpou, 2001), For $\forall \varepsilon_i, \varpi_i \in \mathcal{R}^+$, we have*

$$0 \leqslant |\varpi_i| - \varpi_i \tanh \varpi_i = |\varpi_i| - \varpi_i \tanh\left(\varpi_i/\varepsilon_i\right) \leqslant 0.2785\varepsilon_i,$$

where $i = 1, 2$.

Lemma 2. *The radial basis function neural network (RBFNN) has been confirmed to have a great performance on approximating the unknown function. It can be described as:*

$$f_n(Z) = W^{*T} H(Z) + \varepsilon,$$

where $Z \in \mathcal{R}^+$ is the input data, $H(Z) = [h_1(z), h_2(z), \ldots, h_n(z)]^T$ is the basis function vector, where it can be chosen as:

$$H_q(x) = \exp\left(-\frac{\left\|x - c_j\right\|^2}{2b_j^2}\right), j = 1, 2, \ldots, n,$$

ε is the error of the approximation function.

2.2. Virtual leader–follower model

The formation model based on the leader–follower has been proposed in research (Wang and Li, 2020; Wang et al., 2020b). In this paper, to simplify the leader-follower structure, a virtual leader–follower structure is defined in Fig. 1 referred to (Chen et al., 2020). This figure presents the basic geometric structure of the two ships based on the virtual leader–follower approach, where $X_E - Y_E$ denotes the earth-fixed frame, $x - y$ stands for the body-fixed frame. (x_L, y_L, ψ_L), (x_d, y_d, ψ_d), and (x, y, ψ) represent the position and heading angle of the leadership, virtual ship, and the follower ship, separately. (u_L, v_L, r_L), (u_d, v_d, r_d), and (u, v, r) are their surge, sway, and yaw velocities. The

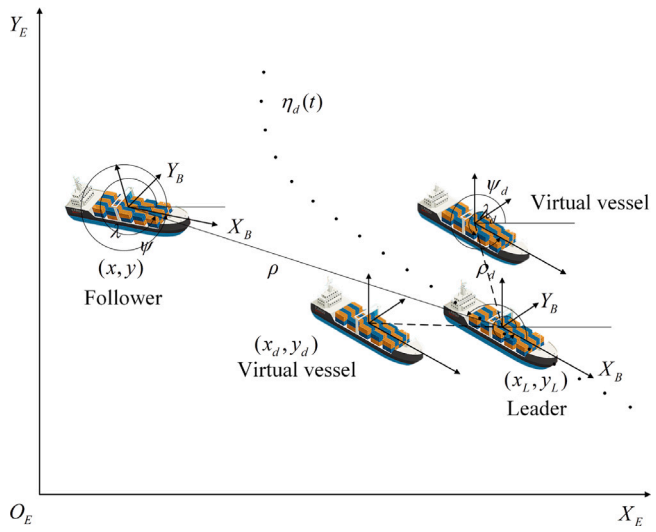

Fig. 1. The formation structure of the leader–follower approach.

formation structure can be constrained by distance ρ and relative angle λ. Thus, we have

$$\begin{aligned} \rho &= \sqrt{\left(x_L - x\right)^2 + \left(y_L - y\right)^2} \\ \lambda &= \arctan\left(y_L - y, x_L - x\right). \end{aligned} \tag{3}$$

Suppose the virtual vessel can keep the formation structure strictly in real-time. If the follower can track the virtual vessel, the desired formation can be completed. Thus, the follower position can be calculated by:

$$\begin{pmatrix} x_d \\ y_d \\ \psi_d \end{pmatrix} = \begin{pmatrix} x_L \\ y_L \\ \psi_L \end{pmatrix} + \begin{pmatrix} \cos(\psi_L) & -\sin(\psi_L) & 0 \\ \sin(\psi_L) & \cos(\psi_L) & 0 \\ 0 & 0 & 1 \end{pmatrix} \begin{pmatrix} \rho_d \cos(\lambda_d) \\ \rho_d \sin(\lambda_d) \\ \beta \end{pmatrix}, \tag{4}$$

where β is the heading angle error between the follower and the virtual vessel.

Remark 2.2. The leadership's position and heading angle (x_L, y_L, ψ_L) and formation structure parameters (ρ_d, λ_d) and β are known.

Assumption 2.1. The variables of following ship including (x, y, ψ), (u, v, r) and their first derivative and second derivative are all smooth bounded.

Thus, the error of the virtual follower's position in the earth-fixed system is given by:

$$\begin{cases} x_e = x - x_d \\ y_e = y - y_d \\ \psi_e = \psi - \psi_d. \end{cases} \tag{5}$$

If the $x = x_d, y = y_d, \psi = \psi_d$, which means $\rho = \rho_d, \lambda = \lambda_d$, and the desired formation structure is achieved. Thus, the formation control problem can be transformed into a trajectory tracking problem.

2.3. Controller objectives

Under the assumptions, the formation control target can be divided into two parts.

Kinematics goal. In earth-fixed coordination, given the desired formation structure ρ_d and λ_d, choose suitable virtual ship speed control law α_u and α_v to ensure $\rho \to \rho_d$ and $\lambda \to \lambda_d$.

Kinetics goal. For kinetics goal, choose suitable input torques τ_u and τ_v to ensure the follower can achieve $u \to \alpha_u$ and $v \to \alpha_v$.

3. Preliminary controller design and stability analysis

In this section, a preliminary formation controller based on the virtual leader–follower approach is introduced. Based on the analysis in Section 2.3, the kinematics and kinetics of the formation system are designed respectively. Moreover, considering the underactuated characteristics and calculation complexity, some innovations are proposed to improve control effectiveness. The preliminary formation controller in this section is proposed under the following assumptions.

Assumption 3.1. Firstly, the preliminary formation controller ignores the uncertainties of ship dynamics, which means (f_u, f_v, f_r) are neglected. Secondly, the upper bounded disturbances $\tau_{wu}^* > 0, \tau_{wv}^* > 0, \tau_{wr}^* > 0$ in Remark 2.1 are known.

3.1. Kinematics control

To design a suitable controller of the kinematics control in earth-fixed system. Define the Lyapunov function candidate of x_e and y_e as the following:

$$V_1 = \frac{1}{2}x_e^2 + \frac{1}{2}y_e^2, \tag{6}$$

where $V_1 \geq 0$, if and only if $e_x = e_y = 0$, $V_1 = 0$. By using backstepping method, to make sure the $\dot{V}_1$ is negative definite. Comparing to traditional Lyapunov function $\dot{x}_e = -kx_e, \dot{y}_e = -ky_e$, we choose a more reliable structure as

$$\begin{bmatrix}\dot{x}_e \\ \dot{y}_e\end{bmatrix} = \begin{bmatrix}-kx_e/\sqrt{x_e^2 + y_e^2 + C} \\ -ky_e/\sqrt{x_e^2 + y_e^2 + C}\end{bmatrix}, \tag{7}$$

where k and C are constant parameters. Differentiating Eq. (7), we have

$$\dot{V}_1 = x_e\dot{x}_e + y_e\dot{y}_e = -k\left(x_e^2 + y_e^2\right)/\sqrt{x_e^2 + y_e^2 + C} \leq 0. \tag{8}$$

Therefore, the error (x_e, y_e) are asymptotically stable. Thus, the time deviation of the Eq. (7) along with Eq. (1) is

$$\begin{bmatrix}\dot{x}_e \\ \dot{y}_e\end{bmatrix} = \begin{bmatrix}\cos(\psi) & -\sin(\psi) \\ \sin(\psi) & \cos(\psi)\end{bmatrix}\begin{bmatrix}u \\ v\end{bmatrix} - \begin{bmatrix}\dot{x}_d \\ \dot{y}_d\end{bmatrix}. \tag{9}$$

Suppose $u \to \alpha_u$ and $v \to \alpha_v$, thus, the virtual control law α_u and α_v are given as:

$$\begin{bmatrix}\alpha_u \\ \alpha_v\end{bmatrix} = \begin{bmatrix}\cos(\psi) & \sin(\psi) \\ -\sin(\psi) & \cos(\psi)\end{bmatrix}\begin{bmatrix}\dot{x}_d - kx_e/\sqrt{x_e^2 + y_e^2 + C} \\ \dot{y}_d - ky_e/\sqrt{x_e^2 + y_e^2 + C}\end{bmatrix}. \tag{10}$$

Define $w = \sqrt{x_e^2 + y_e^2 + C}$, Eq. (10) can be rewritten as:

$$\begin{bmatrix}\alpha_u \\ \alpha_v\end{bmatrix} = \begin{bmatrix}\cos(\psi) & \sin(\psi) \\ -\sin(\psi) & \cos(\psi)\end{bmatrix}\begin{bmatrix}\dot{x}_d - kx_e w^{-1} \\ \dot{y}_d - ky_e w^{-1}\end{bmatrix}, \tag{11}$$

and the derivative of Eq. (11) is

$$\begin{bmatrix}\dot{\alpha}_u \\ \dot{\alpha}_v\end{bmatrix} = \begin{bmatrix}-r\sin(\psi) & r\cos(\psi) \\ -r\cos(\psi) & -r\sin(\psi)\end{bmatrix}\begin{bmatrix}\dot{x}_d - kw^{-1}x_e \\ \dot{y}_d - kw^{-1}y_e\end{bmatrix} + \begin{bmatrix}\cos(\psi) & \sin(\psi) \\ -\sin(\psi) & \cos(\psi)\end{bmatrix}\begin{bmatrix}\ddot{x}_d - k\left(w^{-1} - w^{-3}x_e^2\right)\dot{x}_e + kw^{-3}x_e y_e \dot{y}_e \\ \ddot{y}_d - k\left(w^{-1} - w^{-3}y_e^2\right)\dot{y}_e + kw^{-3}x_e y_e \dot{x}_e\end{bmatrix}. \tag{12}$$

Let

$$\begin{aligned} f = &\left(\ddot{y}_d - k\left(w^{-1} - w^{-3}y_e^2\right)\dot{y}_e + kw^{-3}x_e y_e \dot{x}_e\right)\cos(\psi) \\ &- \left(\ddot{x}_d - k\left(w^{-1} - w^{-3}x_e^2\right)\dot{x}_e + kw^{-3}x_e y_e \dot{y}_e\right)\sin(\psi). \end{aligned} \tag{13}$$

Thus, we have

$$\ddot{\alpha}_v = -\dot{r}\alpha_u - r\dot{\alpha}_u + \dot{f}. \tag{14}$$

3.2. Kinetics control

As the virtual control law of (x_e, y_e) has been established, the next step is to design the control law of (τ_u, τ_r) to realize the tracking of virtual speed control. By using the sliding model control and backstepping method, the lateral motion control τ_r and the surge motion control τ_u are developed.

3.2.1. Surge control law

Define the error of surge motion:

$$u_e = u - \alpha_u. \tag{15}$$

Since the virtual speed can guarantee the stability of the tracking error of body-fixed coordinate, the error of surge error is used to represent the position variables. Hence, define the PI sliding surface as follows

$$S_1 = u_e + \lambda_1 \int_0^t u_e(\tau)\mathrm{d}\tau, \tag{16}$$

where λ_1 is a positive constant. The time derivative along Eq. (16) is presented

$$\begin{aligned} \dot{S}_1 &= \dot{u} - \dot{\alpha}_u + \lambda_1 u_e \\ &= \frac{m_{22}}{m_{11}}vr - \frac{d_{11}}{m_{11}}u + \frac{\tau_u + \tau_{wu}}{m_{11}} - \dot{\alpha}_u + \lambda_1 u_e, \end{aligned} \tag{17}$$

choose $\dot{S}_1 = 0$, we have

$$\tau_{\mathrm{ueq}} = -m_{22}vr + d_{11}u + m_{11}\dot{\alpha}_u - \lambda_1 m_{11}u_e. \tag{18}$$

By choosing a suitable Lyapunov function candidate, the control law can reach the sliding surface in a finite time. Thus, choosing a reaching-law as:

$$\tau_{\mathrm{usw}} = -K_1 \mathrm{sgn}\left(S_1\right), \tag{19}$$

where the sign function is presented as:

$$\mathrm{sgn}(a) = \begin{cases} 1, & a > 0 \\ 0, & a = 0 \\ -1, & a < 0. \end{cases} \tag{20}$$

Thus, the total surge input is $\tau_u = \tau_{\mathrm{ueq}} + \tau_{\mathrm{usw}}$.

Defining the Lyapunov function

$$V_2 = \frac{1}{2}m_{11}S_1^2, \tag{21}$$

and the time derivative of Eq. (21) along with the solution Eq. (17) satisfies

$$\begin{aligned} \dot{V}_2 &= m_{11}S_1\dot{S}_1 \\ &= m_{11}S_1\left(\frac{m_{22}}{m_{11}}vr - \frac{d_{11}}{m_{11}}u + \frac{\tau_u + \tau_{wu}}{m_{11}} - \dot{\alpha}_u + \lambda_1 u_e\right) \\ &\leqslant \tau_{wu}\left|S_1\right| - K_1\left|S_1\right|, \end{aligned} \tag{22}$$

where if choosing $K_1 = \eta_1 + \tau_{wu}^*$, and η_1 is a positive parameter. Thus, we have

$$\dot{V}_2 \leqslant -\eta_1\left|S_1\right|. \tag{23}$$

3.2.2. Sway motion control

Similar to the surge motion control, the error of lateral tracking is defined as

$$v_e = v - \alpha_v, \tag{24}$$

and the sliding surface is selected as:

$$S_2 = \dot{v}_e + \lambda_2 v_e. \tag{25}$$

Differentiating Eq. (25) with Eqs. (1), (10)–(14), we have

$$\begin{aligned} \dot{S}_2 &= \dot{v} - \ddot{\alpha}_v + \lambda_2\left(\dot{v} - \dot{\alpha}_v\right) \\ &= \left(\left(m_{22}\alpha_u - m_{11}u\right)\left(\tau_r + \tau_{wr}\right) - h\right)/m_{22}m_{33}, \end{aligned} \tag{26}$$

where

$$h = -m_{11}m_{33}\dot{u}r - m_{11}u\left(\left(m_{11}-m_{22}\right)uv - d_{33}r\right) - m_{33}d_{22}\dot{v} + m_{33}\dot{\tau}_{wr} + m_{22}\alpha_u\left(\left(m_{11}-m_{22}\right)uv - d_{33}r\right) + m_{22}m_{33}\left(r\dot{\alpha}_u - \dot{f} + \lambda_2\left(\dot{v}-\dot{\alpha}_v\right)\right). \tag{27}$$

Suppose the $\dot{S}_2 = 0$, we have

$$\tau_{req} = h/b, \tag{28}$$

where $b = m_{22}\alpha_u - m_{11}u$, a suitable switch control law is selected as:

$$\tau_{rsw} = -k_2\mathrm{sgn}(S_2). \tag{29}$$

Thus, the lateral motion control law is proposed

$$\tau_r = \tau_{req} + \tau_{rsw} = (h - K_2\mathrm{sgn}(S_2))/b. \tag{30}$$

For most surface vessels, $m_{22} \geqslant 120\%m_{11}$ referred to (Gao, 2006). Thus, we suppose $b > 0$. To ensure the stability of v_e, a Lyapunov candidate is defined as:

$$V_3 = \frac{1}{2}m_{22}m_{33}S_2^2. \tag{31}$$

Differentiating Eq. (31), we have

$$\dot{V}_3 = m_{22}m_{33}S_2\dot{S}_2 = m_{22}m_{33}S_2\left(\left(b\tau_r + b\tau_{wr} - h\right)/m_{22}m_{33}\right) = S_2\left(-K_2\,\mathrm{sgn}\left(S_2\right) + b\tau_{wr}\right). \tag{32}$$

To ensure $\dot{V}_3 \leqslant 0$, Control parameter K_2 is designed as

$$K_2 = \eta_2 + B\tau_{wr}^*, \tag{33}$$

where $\eta_2 > 0$, B is the upper bound of b, B is positive parameter. Thus, we have

$$\dot{V}_3 \leqslant -\eta_2\left|S_2\right|. \tag{34}$$

Choosing a whole Lyapunov candidate as:

$$V_4 = V_2 + V_3. \tag{35}$$

Differentiating V_4 with Eqs. (23) and (34), we have

$$\dot{V}_4 = \dot{V}_2 + \dot{V}_3 \leqslant 0, \tag{36}$$

which shows all tracking errors in formation systems are uniformly ultimately bounded.

Moreover, besides tracking the virtual speed of surge and sway direction by using backstepping and sliding mode algorithms, the speed of yaw motion is also analyzed. Define the following Lyapunov candidate function

$$V_5 = \frac{1}{2}m_{33}r^2. \tag{37}$$

Differentiating Eq. (37) along with Eq. (1)

$$\dot{V}_5 = r((m_{11}-m_{22})uv - d_{33}r + \tau_r + \tau_{wr}). \tag{38}$$

From Eq. (38), if $\left|d_{33}r\right| > \left|r((m_{11}-m_{22})uv - d_{33}r + \tau_r + \tau_{wr})\right|$ satisfies $\dot{V}_5 < 0$, V_5 is a decreasing function. As $\tau_{wu}, \tau_{wr}, u, v$ are all bounded, when r satisfies $\left|d_{33}r\right| > \left|r((m_{11}-m_{22})uv - d_{33}r + \tau_r + \tau_{wr})\right|$, r is a decreasing function because of V_5. Therefore, the yaw motion speed is proven to be Bounded-Input Bounded-Output (BIBO).

4. Advanced controller design and stability analysis

Since the preliminary formation controller in Section 3 has no consideration of uncertain dynamics and unknown disturbances, we utilize two novel methods to estimate the unknown disturbances and dynamic uncertainties. Firstly, we design an adaptive sliding mode control law to estimate all unknown environment interference under Assumption 4.1. Secondly, the RBFNNs are introduced to approach the high-order unknowns in the ship model.

4.1. Unknown disturbance

4.1.1. Control law design

Assumption 4.1. Based on Assumption 3.1, considering the unknown disturbances that are not easy to be got, assuming that the upper bound $\tau_{wu}^* > 0, \tau_{wv}^* > 0, \tau_{wr}^* > 0$ in Remark 2.1 is unknown for this formation controller.

Thus, a new adaptive law with a correction item is designed to estimate the unknown upper bound of unknown disturbance. By using the same controller design in Eqs. (16) and (18), a new switch control law is choosing as:

$$\tau_{usw1} = -\eta_1 S_1 - \hat{\tau}_{wu}^*\phi\left(S_1\right), \tag{39}$$

where $\hat{\tau}_{wu}^*$ is the estimation of τ_{wu}^*. And $\phi\left(S_1\right) = \tanh(s_1/\varepsilon_1)$. η_1, ε_1 are positive parameters. By using the arc-tangent function to replace the symbolic function, the chattering effect can be eliminated effectively.

Thus, the total input τ_u equals:

$$\tau_{u1} = \tau_{ueq} + \tau_{usw1} = -m_{22}vr + d_{11}u + m_{11}\dot{\alpha}_u - \lambda_1 m_{11}u_e - \eta_1 S_1 - \hat{\tau}_{wu}^*\phi\left(S_1\right). \tag{40}$$

An adaptive law to estimate the unknown disturbance is proposed as:

$$\dot{\hat{\tau}}_{wu}^* = \gamma_1\left(S_1\phi\left(S_1\right) - \sigma_1\left(\hat{\tau}_{wu}^* - \tau_{wu}^0\right)\right), \tag{41}$$

where τ_{wu}^0 is the prior estimate of $\hat{\tau}_{wu}^*$, γ_1, σ_1 are positive design parameters.

By using the same controller design in Eq. (39), another adaptive switch control law for yaw motion is selected as:

$$\tau_{rsw1} = -\eta_2 S_2 - \hat{\tau}_{wr}^*\phi\left(S_2\right). \tag{42}$$

Thus, the total input of yaw motion is selected as:

$$\tau_{r1} = \tau_{req} + \tau_{rsw1} = h/b - \eta_2 S_2 - \hat{\tau}_{wr}^*\phi\left(S_2\right). \tag{43}$$

By using the same adaptive estimation law as τ_{wu}^*, the unknown disturbance is estimated as

$$\dot{\hat{\tau}}_{wr}^* = \gamma_2\left(S_2\phi\left(S_2\right) - \sigma_2\left(\hat{\tau}_{wr}^* - \tau_{wr}^0\right)\right), \tag{44}$$

where, $\hat{\tau}_{wr}^*$ is the estimation of τ_{wr}^*. $\phi\left(S_2\right) = \tanh(S_2/\varepsilon_s)$. $\eta_2, \varepsilon_2, \gamma_2, \sigma_2$ are positive parameters.

4.1.2. Stability analysis

Define the total Lyapunov function as follows

$$V_6 = \frac{1}{2}m_{11}S_1^2 + \frac{1}{2}m_{22}m_{33}S_2^2 + \frac{1}{2\gamma_1}(\tilde{\tau}_{wu}^*)^2 + \frac{1}{2\gamma_2}(\tilde{\tau}_{wr}^*)^2, \tag{45}$$

where $\tilde{\tau}_{wu}^* = \hat{\tau}_{wu}^* - \tau_{wu}^*, \tilde{\tau}_{wr}^* = \hat{\tau}_{wr}^* - \tau_{wr}^*$ are errors of estimations. Differentiating V_6 along with Eq. (39) to Eq. (44), we have Eq. (46)

$$\begin{aligned}
\dot{V}_6 &= m_{11}S_1\dot{S}_1 + m_{22}m_{33}S_2\dot{S}_2 + \frac{1}{\gamma_1}\tilde{\tau}_{wu}^*\dot{\hat{\tau}}_{wu}^* + \frac{1}{\gamma_2}\tilde{\tau}_{wr}^*\dot{\hat{\tau}}_{wr}^* \\
&= S_1\left(-\hat{\tau}_{wu}^*\phi\left(S_1\right) - \eta_1 S_1 + \tau_{wu}\right) \\
&+ S_2\left(-\hat{\tau}_{wr}^*\phi\left(S_2\right) - \eta_2 S_2 + \tau_{wr}\right) + \frac{1}{\gamma_1}\tilde{\tau}_{wu}^*\dot{\hat{\tau}}_{wu}^* + \frac{1}{\gamma_2}\tilde{\tau}_{wr}^*\dot{\hat{\tau}}_{wr}^* \\
&\leqslant -\eta_1 S_1^2 - \eta_2 S_2^2 + \tau_{wu}^*\left|S_1\right| + \tau_{wr}^*\left|S_2\right| - \hat{\tau}_{wu}^* S_1\phi\left(S_1\right) \\
&- \hat{\tau}_{wr}^* S_2\phi\left(S_2\right) + \tilde{\tau}_{wu}^*\left(S_1\phi\left(S_1\right) - \sigma_1\left(\hat{\tau}_{wu}^* - \tau_{wu}^0\right)\right) \\
&+ \tilde{\tau}_{wr}^*\left(S_2\phi\left(S_2\right) - \sigma_2\left(\hat{\tau}_{wt}^* - \tau_{wt}^0\right)\right) \\
&= -\eta_1 S_1^2 - \eta_2 S_2^2 + \tau_{wu}^*\left|S_1\right| + \tau_{wr}^*\left|S_2\right| - \hat{\tau}_{wu}^* S_1\phi\left(S_1\right) \\
&- \hat{\tau}_{wr}^* S_2\phi\left(S_2\right) + \left(\hat{\tau}_{wu}^* - \tau_{wu}^*\right)\left(S_1\phi\left(S_1\right) - \sigma_1\left(\hat{\tau}_{wu}^* - \tau_{wu}^0\right)\right) \\
&+ \left(\hat{\tau}_{wr}^* - \tau_{wt}^*\right)\left(S_2\phi\left(S_2\right) - \sigma_2\left(\hat{\tau}_{wr}^* - \tau_{wt}^0\right)\right) \\
&= -\eta_1 S_1^2 - \eta_2 S_2^2 \\
&+ \tau_{wu}^*\left(\left|S_1\right| - S_1\phi\left(S_1\right)\right) + \tau_{wr}^*\left(\left|S_2\right| - S_2\phi\left(S_2\right)\right) \\
&- \sigma_1\left(\tau_{wu}^* - \hat{\tau}_{wu}^*\right)\left(\hat{\tau}_{wu}^* - \tau_{wu}^0\right) - \sigma_2\left(\tau_{wr}^* - \hat{\tau}_{wr}^*\right)\left(\hat{\tau}_{wr}^* - \tau_{wr}^0\right).
\end{aligned} \tag{46}$$

From Lemma 1, we have

$$\begin{aligned}&|S_1| - S_1\phi(S_1) \leqslant 0.2785\varepsilon_1\\&|S_2| - S_2\phi(S_2) \leqslant 0.2785\varepsilon_2.\end{aligned} \tag{47}$$

Considering $-\left(\hat{\tau}^*_{wu} - \tau^*_{wu}\right)\left(\hat{\tau}^*_{wu} - \tau^0_{wu}\right)$ satisfies

$$-\left(\hat{\tau}^*_{wu} - \tau^*_{wu}\right)\left(\hat{\tau}^*_{wu} - \tau^0_{wu}\right) \leqslant -\frac{1}{2}\left(\hat{\tau}^*_{wu} - \tau^*_{wu}\right)^2 + \frac{1}{2}\left(\tau^*_{wu} - \tau^0_{wu}\right)^2. \tag{48}$$

The similar structure $-\left(\hat{\tau}^*_{wr} - \tau^*_{wr}\right)\left(\hat{\tau}^*_{wr} - \tau^0_{wr}\right)$ satisfies:

$$-\left(\hat{\tau}^*_{wr} - \tau^*_{wr}\right)\left(\hat{\tau}^*_{wr} - \tau^0_{wr}\right) \leqslant -\frac{1}{2}\left(\hat{\tau}^*_{wr} - \tau^*_{wr}\right)^2 + \frac{1}{2}\left(\tau^*_{wr} - \tau^0_{wr}\right)^2. \tag{49}$$

Thus, we can obtain

$$\begin{aligned}\dot{V}_6 \leqslant\ & -\eta_1 S_1^2 - \eta_2 S_2^2 - \frac{\sigma_1}{2}\left(\hat{\tau}^*_{wu} - \tau^*_{wu}\right)^2 + \frac{\sigma_1}{2}\left(\tau^*_{wu} - \tau^0_{wu}\right)^2\\&- \frac{\sigma_2}{2}\left(\hat{\tau}^*_{w\tau} - \tau^*_{wr}\right)^2 + \frac{\sigma_2}{2}\left(\tau^*_{wt} - \tau^0_{wr}\right)^2\\&+ 0.2785\varepsilon_1\tau^*_{wu} + 0.2785\varepsilon_2\tau^*_{wr}\\\leqslant\ & \mu_1 V + C_1,\end{aligned} \tag{50}$$

where

$$\begin{aligned}\mu_1 &= \min(2\eta_1, 2\eta_2, \sigma_1, \sigma_2)\\C_1 &= \frac{\sigma_1}{2}\left(\tau^*_{wu} - \tau^0_{wu}\right)^2\\&+ \frac{\sigma_2}{2}\left(\tau^*_{wt} - \tau^0_{wr}\right)^2 + 0.2785\varepsilon_1\tau^*_{wu} + 0.2785\varepsilon_2\tau^*_{wr}.\end{aligned} \tag{51}$$

From Eq. (50), one concludes that

$$0 \leqslant V_6(t) \leqslant \frac{C_1}{\mu_1} + \left[V_6(0) - \frac{C_1}{\mu_1}\right]e^{-\mu_1 t}, \tag{52}$$

where, V is converged in the sphere whose center is at the origin and radius is C_1/μ_1. As all the signals including $S_1, S_2, \tilde{\tau}^*_{wu}, \tilde{\tau}^*_{wr}$ are uniformly ultimately bounded. Thus, u_e, v_e are bounded, and the estimation $\hat{\tau}^*_{wu}, \hat{\tau}^*_{wr}$ are bounded, which proves that all tracking errors are uniformly ultimately bounded (UUB).

4.2. Uncertain dynamics

4.2.1. Control law design

Besides the consideration of unknown disturbances, the approach to high-order ship dynamics are conducted by using RBFNNs. $f = \left[f_u f_v f_r\right]^{\mathrm{T}}$ represents the uncertainty of ship dynamics, which are totally unknown. By using the same sliding surface in Eq. (16), and the derivation is

$$\begin{aligned}\dot{S}_1 &= \dot{u} - \dot{\alpha}_u + \lambda_1 u_e\\&= \frac{m_{22}}{m_{11}}vr - \frac{d_{11}}{m_{11}}u - \frac{f_u}{m_{11}} + \frac{\tau_u + \tau_{wu}}{m_{11}} - \dot{\alpha}_u + \lambda_1 u_e,\end{aligned} \tag{53}$$

where f_u is the unknown dynamics of the ship model that is not easy to be got. From Lemma 2, we have

$$f_u = W_u^{*\mathrm{T}}h(z) + \varsigma_1, \tag{54}$$

where $z = [u, v, r]^T$ is the input vector of the network. ς_1 is the approximation error which has an upper bound $\varsigma_B > 0$.

Thus, the control law of surge motion is selected as

$$\begin{aligned}\tau_{u2} &= \tau_{ueq1} + \tau_{usw1}\\&= -m_{22}vr + d_{11}u + f_u + m_{11}\dot{\alpha}_u - \lambda_1 m_{11}u_e\\&\quad - \eta_1 S_1 - \hat{\tau}^*_{wu}\phi(S_1)\\&= -m_{22}vr + d_{11}u + W_u^{*\mathrm{T}}h(z) + m_{11}\dot{\alpha}_u - \lambda_1 m_{11}u_e\\&\quad - \eta_1 S_1 - \hat{\tau}^*_{wu}\phi(S_1),\end{aligned} \tag{55}$$

and the adaptive weight design law of RBF neural networks is derived in the sense of the Lyapunov stability theorem by the backstepping method.

$$\dot{\hat{W}}_u = -\Gamma_1\left(S_1 h(z) + \vartheta_1\hat{W}_u\right). \tag{56}$$

For sway speed control, the sliding surface is chosen as Eq. (25) the derivation can is given by:

$$\begin{aligned}\dot{S}_2 &= \ddot{v} + \dot{r}\alpha_u + r\dot{\alpha}_u - \dot{f} + \lambda_2\left(\dot{v} - \dot{\alpha}_v\right)\\&= \ddot{v} + \frac{\alpha_u}{m_{33}}\left(\left(m_{11} - m_{22}\right)uv - d_{33}r - f_r + \tau_r + \tau_{wr}\right)\\&\quad + r\dot{\alpha}_u - \dot{f} + \lambda_2\left(\dot{v} - \dot{\alpha}_v\right),\end{aligned} \tag{57}$$

where f_r is approached by RBFNNs as the following:

$$f_r = W_r^{*\mathrm{T}}h(z) + \varsigma_2. \tag{58}$$

Thus, the yaw input is chosen as:

$$\begin{aligned}\tau_{r2} =\ & -m_{33}\left(\ddot{v} + r\dot{\alpha}_u - \dot{f} + \lambda_2\left(\dot{v} - \dot{\alpha}_v\right)\right)/\alpha_u\\&- \left(m_{11} - m_{22}\right)uv + d_{33}r + \hat{W}_{\mathrm{r}}^{\mathrm{T}}h(z)\\&- \eta_2 S_2 - \hat{\tau}^*_{wr}\phi(S_2).\end{aligned} \tag{59}$$

Similar to Eq. (56), we have

$$\dot{\hat{W}}_{\mathrm{r}} = -\Gamma_2\left(S_2 h(z) + \vartheta_2\hat{W}_{\mathrm{r}}\right). \tag{60}$$

4.2.2. Stability analysis

In this section, a total Lyapunov function is selected to prove the effectiveness of the whole tracking error. Considering the external disturbances and internal unknowns, parameters adaptation formulas Eqs. (41) and (44), and RBFNNs formulas Eqs. (54) and (58) are proposed respectively.

$$\begin{aligned}V_7 &= \frac{1}{2}m_{11}S_1^2 + \frac{1}{2\gamma_1}(\tilde{\tau}^*_{wu})^2 + \frac{1}{\Gamma_1}\tilde{W}_u^{\mathrm{T}}\tilde{W}_u\\&+ \frac{1}{2}m_{33}S_2^2 + \frac{1}{2\gamma_2}(\tilde{\tau}^*_{wr})^2 + \frac{1}{\Gamma_2}\tilde{W}_r^{\mathrm{T}}\tilde{W}_r,\end{aligned} \tag{61}$$

Estimation of disturbances bound error and weight error are defined as

$$\begin{aligned}&\tilde{\tau}^*_{wu} = \tau^*_{wu} - \hat{\tau}^*_{wu}, \tilde{\tau}^*_{wr} = \tau^*_{wr} - \hat{\tau}^*_{wr}\\&\tilde{W}_u = \hat{W}_u - W_u^*, \tilde{W}_r = \hat{W}_r - W_r^*.\end{aligned} \tag{62}$$

Differentiating Eq. (61) along with Eqs. (53), (57), (56), and (60), we have (see Box I).

Considering the following reasons: Firstly, from Lemma 1 in Eq. (47), we have

$$|S_1| - S_1\phi(S_1) \leqslant 0.2785\varepsilon_1, \tag{64}$$

Secondly, the inequality shows that

$$\begin{aligned}&-\varsigma_1 S_1 \leqslant \frac{S_1^2}{2} + \frac{S_1^2}{2} \leqslant \frac{\varsigma_{\mathrm{U}}^2}{2} + \frac{S_1^2}{2}\\&\left(\tau^*_{wu} - \hat{\tau}^*_{wu}\right)\left(\hat{\tau}^*_{wu} - \tau^0_{wu}\right) \leqslant -\frac{1}{2}\left(\hat{\tau}^*_{wu} - \tau^*_{wu}\right)^2 + \frac{1}{2}\left(\tau^*_{wu} - \tau^0_{wu}\right)^2\\&-\vartheta_1\tilde{W}_u^{\mathrm{T}}\hat{W}_u = -\vartheta_1\tilde{W}_u^{\mathrm{T}}\left(\tilde{W}_u + W_u^*\right) \leqslant -\frac{\vartheta_1}{2}\tilde{W}_u^{\mathrm{T}}\tilde{W}_u + \frac{\vartheta_1}{2}W_{\mathrm{U}}^2.\end{aligned} \tag{65}$$

Meanwhile, the structure of sway motion can be derived according to the same form. Thus, Eq. (63) is rewritten as:

$$\begin{aligned}\dot{V}_7 \leqslant\ & -\eta_1 S_1^2 - \eta_2 S_2^2 + 0.2785\varepsilon_1\tau^*_{wu} + 0.2785\varepsilon_2\tau^*_{wr} + \frac{\varsigma_{\mathrm{U}}}{2}\\&+ \frac{S_1^2}{2} + \frac{\varsigma_{\mathrm{R}}^2}{2} + \frac{S_2^2}{2} - \frac{\sigma_1}{2}\left(\hat{\tau}^*_{wu} - \tau^*_{wu}\right)^2 + \frac{\sigma_1}{2}\left(\tau^*_{wu} - \tau^0_{wu}\right)^2\\&- \frac{\sigma_2}{2}\left(\hat{\tau}^*_{wr} - \tau^*_{wr}\right)^2 + \frac{\sigma_2}{2}\left(\tau^*_{wr} - \tau^0_{wr}\right)^2\\&- \frac{\vartheta_1}{2}\tilde{W}_u^{\mathrm{T}}\tilde{W}_u + \frac{\vartheta_1}{2}\left\|W_u^*\right\|^2 - \frac{\vartheta_2}{2}\tilde{W}_{\mathrm{r}}^{\mathrm{T}}\tilde{W}_{\mathrm{r}} + \frac{\vartheta_2}{2}\left\|W_{\mathrm{r}}^*\right\|^2\\=\ & -\frac{2\eta_1 - 1}{2}S_1^2 - \frac{2\eta_2 - 1}{2}S_2^2 - \frac{\sigma_1}{2}\left(\hat{\tau}^*_{wu} - \tau^*_{wu}\right)^2\\&- \frac{\sigma_2}{2}\left(\hat{\tau}^*_{wr} - \tau^*_{wr}\right)^2 + \frac{\varsigma_{\mathrm{U}}^2}{2} + \frac{\varsigma_{\mathrm{R}}^2}{2} + 0.2785\varepsilon_1\tau^*_{wu}\\&+ 0.2785\varepsilon_2\tau^*_{wr} + \frac{\sigma_1}{2}\left(\tau^*_{wu} - \tau^0_{wu}\right)^2 + \frac{\sigma_2}{2}\left(\tau^*_{wr} - \tau^0_{wr}\right)^2\\&- \frac{\vartheta_1}{2}\tilde{W}_u^{\mathrm{T}}\tilde{W}_u - \frac{\vartheta_2}{2}\tilde{W}_{\mathrm{r}}^{\mathrm{T}}\tilde{W}_{\mathrm{r}} + \frac{\vartheta_1}{2}W_{\mathrm{U}}^2 + \frac{\vartheta_2}{2}W_{\mathrm{R}}^2\\\leqslant\ & -\mu_2 V + C_2.\end{aligned} \tag{66}$$

$$
\begin{aligned}
\dot{V}_7 &= m_{11}S_1\dot{S}_1 + m_{33}S_2\dot{S}_2 - \frac{1}{\gamma_1}\tilde{\tau}_{wu}\dot{\hat{\tau}}^*_{wu} - \frac{1}{\gamma_2}\tilde{\tau}^*_{wr}\dot{\hat{\tau}}^*_{wr} + \frac{1}{\Gamma_1}\tilde{W}_u^{\mathrm{T}}\dot{\hat{W}}_u + \frac{1}{\Gamma_2}\tilde{W}_{\mathrm{r}}^{\mathrm{T}}\dot{\hat{W}}_{\mathrm{r}} \\
&= S_1\left(\tilde{W}_u^{\mathrm{T}}h(z) - \varsigma_1 - \eta_1 S_1 + \tau^*_{wu} - \hat{\tau}^*_{wu}\phi\left(S_1\right)\right) + S_2\left(\tilde{W}_{\mathrm{r}}^{\mathrm{T}}h(z) - \varsigma_2 - \eta_2 S_2 + \tau^*_{wr} - \hat{\tau}^*_{wr}\phi\left(S_2\right)\right) \\
&- \tilde{\tau}^*_{wu}\left(S_1\phi\left(S_1\right) - \sigma_1\left(\hat{\tau}^*_{wu} - \tau^0_{wu}\right)\right) - \tilde{\tau}^*_{wr}\left(S_2\phi\left(S_2\right) - \sigma_2\left(\hat{\tau}^*_{wr} - \tau^0_{wr}\right)\right) \\
&- \tilde{W}_u^{\mathrm{T}}h(z)S_1 - \vartheta_1\tilde{W}_u^{\mathrm{T}}\hat{W}_u - \tilde{W}_{\mathrm{r}}^{\mathrm{T}}h(z)S_2 - \vartheta_2\tilde{W}_{\mathrm{r}}^{\mathrm{T}}\hat{W}_{\mathrm{r}} \\
&\leqslant -\eta_1 S_1^2 - \eta_2 S_2^2 + \tau^*_{wu}\left(\left|S_1\right| - S_1\phi\left(S_1\right)\right) + \tau^*_{wr}\left(\left|S_2\right| - S_2\phi\left(S_2\right)\right) - \varsigma_1 S_1 - \varsigma_2 S_2 \\
&+ \sigma_1\left(\tau^*_{wu} - \hat{\tau}^*_{wu}\right)\left(\hat{\tau}^*_{wu} - \tau^0_{wu}\right) + \sigma_2\left(\tau^*_{wr} - \hat{\tau}^*_{wr}\right)\left(\hat{\tau}^*_{wr} - \tau^0_{wr}\right) - \vartheta_1\tilde{W}_u^{\mathrm{T}}\hat{W}_u - \vartheta_2\tilde{W}_{\mathrm{r}}^{\mathrm{T}}\hat{W}_{\mathrm{r}}.
\end{aligned}
\tag{63}
$$

Box I.

Table 1
Parameters of isomorphic formation simulation. (These isomorphic ship parameters are referred to in Do et al., 2004; Shen, 2019.)

Ship	Ship parameters $(m_{11}, m_{22}, m_{33}, d_{11}, d_{22}, d_{33})$	Initial status (x, y, ψ, u, v, r)	Formation structure (ρ_d, λ_d)
Leader	$(1.2\times10^5, 1.779\times10^5, 6.36\times10^7, 2.15\times10^4, 1.47\times10^5, 8.02\times10^6)$	(0,0,0,−10,300,0)	–
Follower1	$(1.2\times10^5, 1.779\times10^5, 6.36\times10^7, 2.15\times10^4, 1.47\times10^5, 8.02\times10^6)$	(0,0,0,−30,320,0)	$(20, \pi/2)$
Follower2	$(1.2\times10^5, 1.179\times10^5, 6.36\times10^7, 2.15\times10^4, 1.17\times10^5, 8.02\times10^6)$	(0,0,0,−40,270,0)	$(20, -\pi/2)$

Table 2
The environmental disturbances and ship uncertainties of isomorphic formation simulation.

$\tau_{wu} = 10^4\,[\sin(0.2t) + \cos(0.5t)]$	$\tau_{wv} = 10^2\,[\sin(0.1t) + \cos(0.4t)]$	$\tau_{wr} = 10^5\,[\sin(0.5t) + \cos(0.3t)]$
$f_u = 0.2d_{11}u^2 + 0.1d_{11}u^3$	$f_v = 0.2d_{22}v^2 + 0.1d_{22}v^3$	$f_r = 0.2d_{33}r^2 + 0.1d_{33}r^3$

As a result, Eq. (66) can be rewritten as

$$
0 \leqslant V_{(t)} \leqslant \frac{C_2}{\mu_2} + \left(V_{(0)} - \frac{C_2}{\mu_2}\right)e^{-\mu_2 t}, \tag{67}
$$

where

$$
\begin{aligned}
\mu_2 &= \min(2\eta_1 - 1, 2\eta_2 - 1, \sigma_1, \sigma_2, \vartheta_1, \vartheta_2) \\
C_2 &= \frac{\zeta_{\mathrm{U}}^2}{2} + \frac{\zeta_{\mathrm{R}}^2}{2} + 0.2785\varepsilon_1\tau^*_{wu} + 0.2785\varepsilon_2\tau^*_{wr} \\
&+ \frac{\sigma_1}{2}\left(\tau^*_{wu} - \tau^0_{wu}\right)^2 + \frac{\sigma_2}{2}\left(\tau^*_{wr} - \tau^0_{wr}\right)^2 \\
&+ \frac{\vartheta_1}{2}W_{\mathrm{U}}^2 + \frac{\vartheta_2}{2}W_{\mathrm{R}}^2.
\end{aligned}
\tag{68}
$$

Thus, V is converged in the sphere whose center is at the origin and radius is C_2/μ_2. As all the signals including $S_1, S_2, \tilde{\tau}^*_{wu}, \tilde{\tau}^*_{wr}, \tilde{W}_u, \tilde{W}_r$ are uniformly ultimately bounded, which proves that u_e, v_e are bounded, and the error of position x_e, y_e are bounded, which proves that all tracking errors are uniformly ultimately bounded (UUB).

5. Results and discussion

In this section, related experiments are executed in MATLAB R2020b on a PC that has an I7-9750H CPU and 16 GB memory. Numerical simulations are carried out to demonstrate the efficiency and effectiveness of the proposed formation controller for multiple vessels. Firstly, we compare the controller performance with other existing controllers on leader tracking control, which shows that the proposed method has a better performance. Meanwhile, for formation control verification, isomorphic simulations are demonstrated by using the same ship parameters and target trajectory. Furthermore, to extend the scope of application on multiple ship formation navigation in cargo delivery, heterogeneous ships are introduced to show that the proposed method is highly adaptable for different characteristics.

To verify the effectiveness of the proposed method, larger ships rather than small USVs are considered as a suitable simulation object. Detailed information of these ships are given in Tables 1 and 5. The environmental disturbances and ship uncertainties are assumed unknown but bounded, where the time-varying disturbances are defined in Table 2.

Table 3
Control parameters of proposed SMC algorithms.

$k = 1.8$	$C = 1$	$\lambda_1 = 1$
$\lambda_2 = 1$	$\varepsilon_1 = 0.1$	$\varepsilon_2 = 0.1$
$\eta_1 = 1\times10^4$	$\eta_2 = 1\times10^4$	$\Gamma_1 = 1\times10^5$
$\vartheta_1 = 1\times10^{-8}$	$\Gamma_1 = 1\times10^5$	$\vartheta_1 = 1\times10^{-8}$
$\gamma_1 = 8\times10^4$	$\gamma_2 = 8\times10^5$	$\sigma_1 = 0.8\times10^{-7}$
$\sigma_2 = 1.5\times10^{-8}$	$\tau^0_{wu} = 0.1$	$\tau^0_{wr} = 0.1$

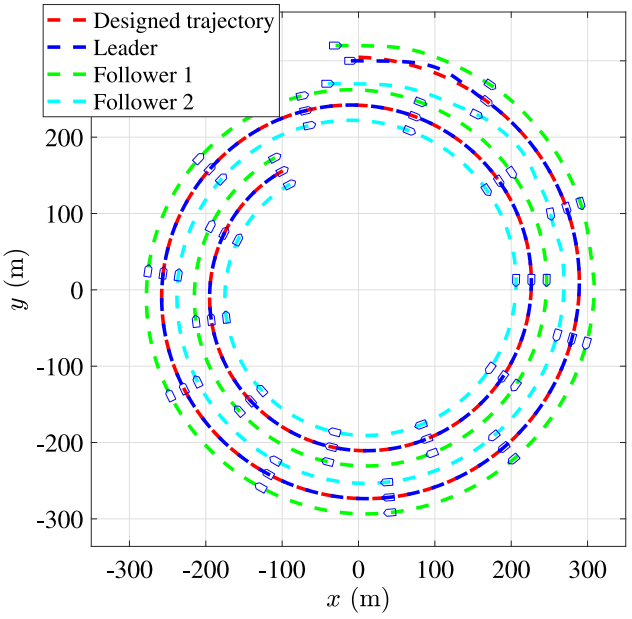

Fig. 2. The performance of the tracking and formation control.

5.1. Controller comparison and isomorphic formation simulations

In this part, three isomorphic ships in a virtual leader–follower formation structure are considered by using the same parameters. The

Table 4
Controller performance comparison of position tracking error η_e.

Switch control law	MSE	RMSE	MAE	MAPE	SMAPE	R2
The propose controller	0.8830	0.9397	0.1901	6.3535e−4	0.0638	0.9993
$\tau_{usw} = -\hat{\tau}^*_{wu}\,\mathrm{sgn}(S_1)\,\lvert S_1\rvert^{\alpha}$	1.55474	1.2449	0.3097	0.0010	0.1040	0.9987
$\tau_{rsw} = -\hat{\tau}^*_{wr}\,\mathrm{sgn}(S_2)\,\lvert S_2\rvert^{\alpha}$	1.2575	1.1214	0.2825	9.5321e−4	0.0954	0.9990
Both switch control laws changed	1.0732	1.0359	0.2607	8.8174e−4	0.0882	0.9991

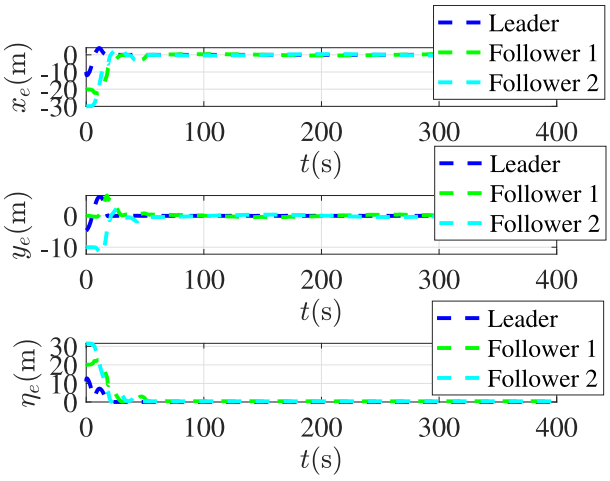

Fig. 3. The kinematics errors of the follower and leadership.

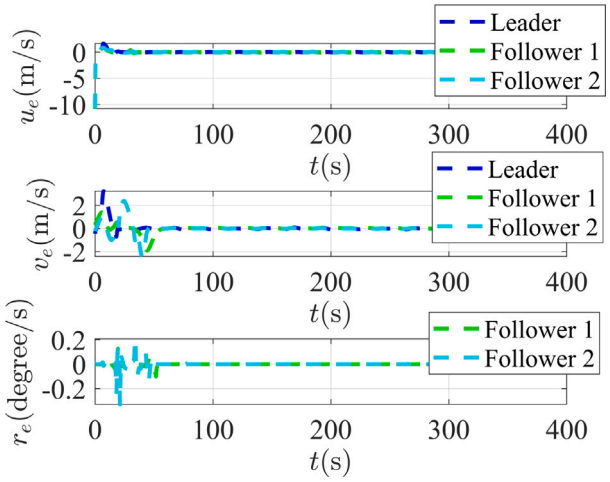

Fig. 4. The kinetics errors of the follower and leadership.

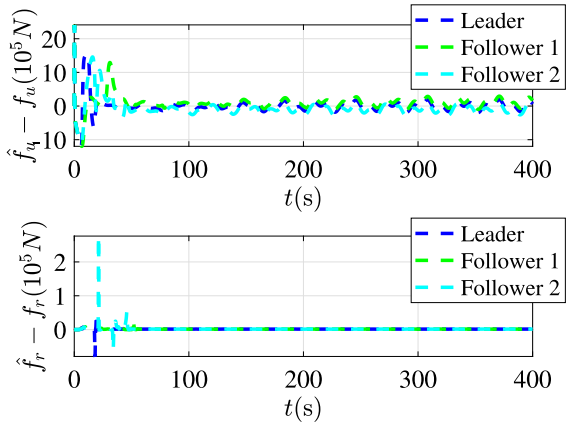

Fig. 5. The approximation values of the ship uncertain dynamics between leader and followers.

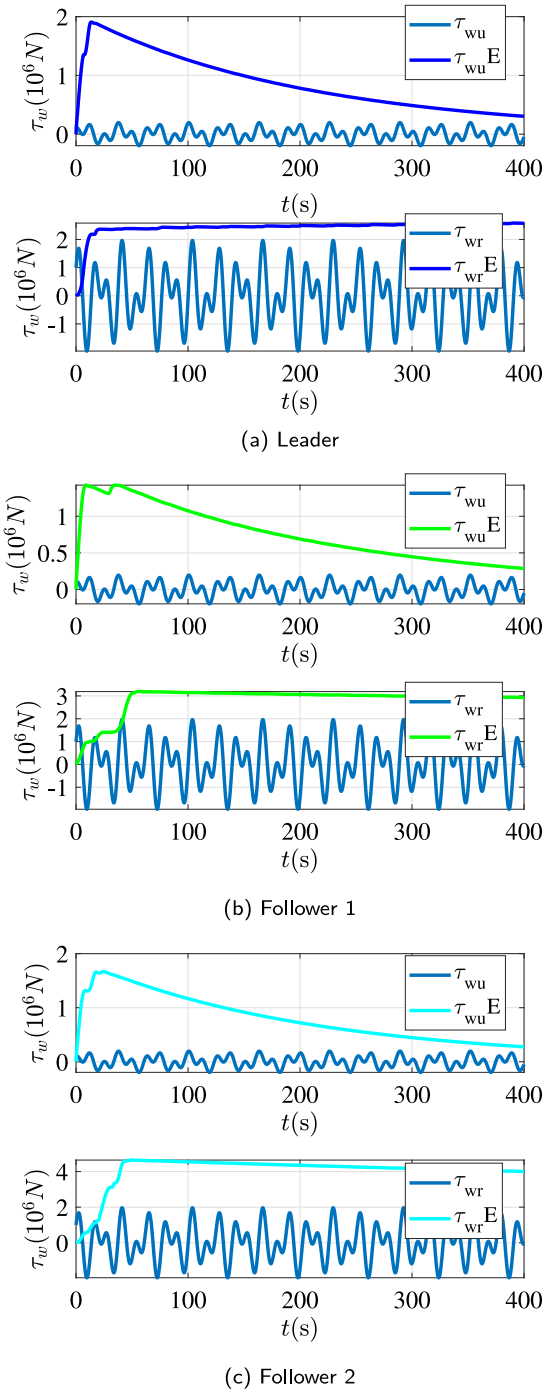

Fig. 6. The estimation of the upper bound on external disturbances.

formation configuration is set in Table 1. And the control parameters are given in Table 3.

Compare to another fixed-time terminal sliding mode controller referred in (Bhat and Bernstein, 2000; Polyakov, 2011), that is the

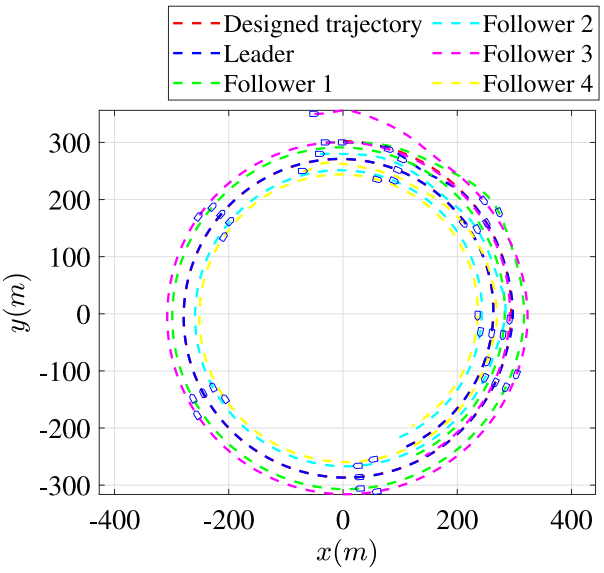

Fig. 7. The performance of the tracking and formation control in Route 1.

switch control law is chosen as $\tau_{sw} = -p^* \mathrm{sgn}\left(S_1\right)|S_1|^{\alpha}$. According to the equation mentioned before, we choose $p = \hat{\tau}^*_{wu}$ *or* $\hat{\tau}^*_{wr}, \alpha = 1/3$. Table 4 shows the results of the tracking errors. In this comparison, the fixed-time terminal sliding mode controller is verified to be more effective in either or both control inputs (τ_u or τ_r).

MAE (Mean Absolute Error), RMSE (Root Mean Square Error), MAE (Mean Absolute Error), MAPE (Mean Absolute Percentage Error), and SMAPE (Symmetric Mean Absolute Percentage Error) are used to evaluate the average of the errors in different aspects, while R2 (R-squared) indicates the proportion of the variation in the dependent variable that is predictable from the independent variables. From Table 4, the R2 of the proposed controller is the law closest to 1, meanwhile, other measurements are closest to zero, which shows that the proposed controller has a better performance on the tracking problem.

To further verify the feasibility of the trajectory of the whole formation structure, we used the trajectory tacking control method for the leadership to follow instead of changing inputs $(\tau_u, 0, \tau_r)$ directly, which is neglected in previous research. By using the leader's tracking routes, the followers can have a more real and feasible tracking paths. The desired trajectory for leadership is given as $xd = 300(1 - 0.001(t - 15.7))sin(0.03t)$; $yd = 300(1 - 0.001(t - 15.7))cos(0.03t)$; referred in (Jin et al., 2021), and the tracking control method is the same as the proposed formation tracking control method. Thus, as the leadership is tracking the desired routes, the virtual followers' position is determined by the formation scheme, and the followers start maintaining the formation structure.

Formation results are shown in Figs. 2–6. The reference trajectories and formation trajectories are presented in Fig. 2, indicates that desired trajectory and formation trajectories could be tracked by a leader and followers despite the existence of the model uncertainties and external disturbances. Figs. 3 and 4 proves that both position errors and velocity errors ultimately smoothly converged to a small neighborhood of zero, which demonstrates the effectiveness of the proposed formation scheme. Figs. 5 and 6 illustrates the learning ability and the estimation ability for external disturbances and model uncertainties respectively. Both leader and followers can have effective performance on approximation and estimation for surge and yaw motion.

5.2. Heterogeneous formation simulations

In this section, more heterogeneous ships and simulations are added to verify the effectiveness of the proposed formation scheme. As almost every ship has its own maneuverability, thus, several heterogeneous ship models are introduced in Table 5, and their initial status and formation structures are proposed as well. Other parameters are listed

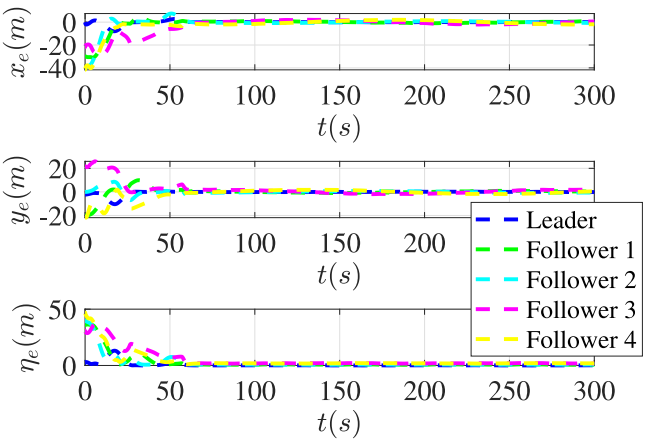

Fig. 8. The kinematics errors of the follower and leadership in Route 1.

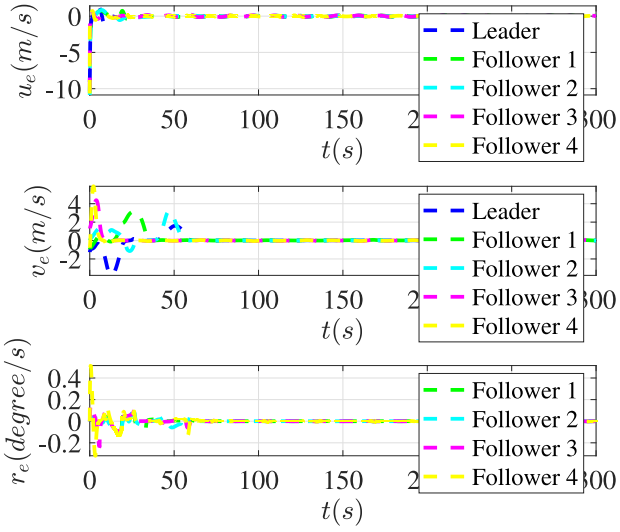

Fig. 9. The kinetics errors of the follower and leadership in Route 1.

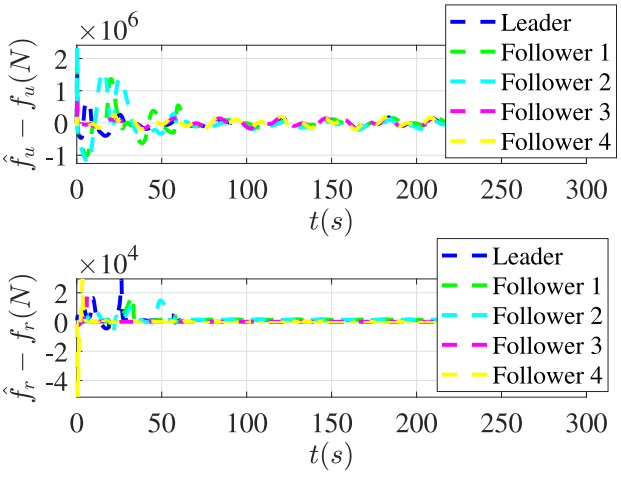

Fig. 10. The approximation values errors of the ship uncertain dynamics between leader and followers in Route 1.

Table 5
Parameters of heterogeneous formation simulation. (The Leader, Follower1 and Follower2 are referred to in Do et al., 2004; Shen, 2019, and the rest followers are designed by reducing the order of magnitude of parameters.)

Ship	Ship parameters $(m_{11}, m_{22}, m_{33}, d_{11}, d_{22}, d_{33})$	Initial status (x, y, ψ, u, v, r)	Formation structure (ρ_d, λ_d)
Leader	$(1.2\times10^5, 1.779\times10^5, 6.36\times10^7, 2.15\times10^4, 1.47\times10^5, 8.02\times10^6)$	(0,0,0,0,300,0)	–
Follower1	$(1.2\times10^5, 1.779\times10^5, 6.36\times10^7, 2.15\times10^4, 1.47\times10^5, 8.02\times10^6)$	(0,0,0,−30,300,0)	$(20, \pi/2)$
Follower2	$(1.2\times10^5, 2.179\times10^5, 6.36\times10^7, 2.15\times10^4, 1.17\times10^5, 8.02\times10^6)$	(0,0,0,−40,−280,0)	$(20, -\pi/2)$
Follower3	$(1.2\times10^4, 1.779\times10^4, 6.36\times10^6, 2.15\times10^3, 1.47\times10^4, 8.02\times10^5)$	(0,0,0,−50,350,0)	$(40, 3\pi/4)$
Follower4	$(1.2\times10^3, 1.779\times10^3, 6.36\times10^5, 2.15\times10^3, 1.47\times10^4, 8.02\times10^4)$	(0,0,0,−70,250,0)	$(40, -3\pi/4)$

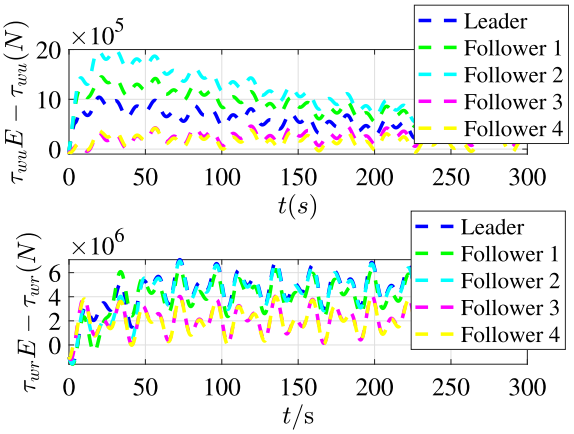

Fig. 11. The estimation of the upper bound error on external disturbances in Route 1.

in Section 5.1. To verify the adaptability of the proposed formation controller on heterogeneous ships, besides the previously mentioned trajectory as the Route 1, a new figure-8 curve, $x_d = 300\sin(0.03t); y_d = 200\sin(0.06(t + pi/2))$ as Route 2, is introduced as the leader trajectory reference.

For comparison purposes, the first heterogeneous formation experiment results based on Route 1 are shown in Figs. 7–11 where the last two heterogeneous ships (Follower 3 and Follower 4) can keep the formation tracking as well as the two isomorphic ships (Follower 1 and Follower 2).

Remark 5.1. With the decrease in radius of the designed trajectory, it is normal for the leader ship and the follower ships to have some fluctuations in the kinetics tracking errors. The kinematics errors are very small compared to the magnitude of the target routes after these errors become stable. The approximation value errors of the ship uncertain dynamics converge to a neighborhood of zero, which shows that the adaptive law is suitable for this formation scheme. The estimation values are greater than the actual values, and this helps to eliminate the influences of all external disturbances.

Remark 5.2. During the controller simulations, the calculation complexity is mainly due to the online RBFNNs. To ensure the control accuracy as much as possible under the premise of decreasing the complexity, an offline rolling RBFNNs is introduced. The performance of the RBFNNs does not continue to improve as the neurons are added. Thus, the mean squared error goal of RBFNNs is selected by the distance between the initial ship position and desired trajectory. Then, the maximum number of neurons is determined. Secondly, Updating RBFNNs with the data group of the previous period also helps to improve the accuracy. By these methods, the simulation time is decreased.

Compared to the isomorphic ships, the two heterogeneous followers can track the leader by using the same controller structure and parameters. This shows that the proposed controller has a good adaptability for different ships with heterogeneous dynamics.

To better verify the effectiveness and efficiency of the proposed controller, Route 2 is introduced and related results are shown in Figs. 12–16, where we can have some similar results. The reference trajectories and formation trajectories are presented in Fig. 12, which demonstrates that the desired trajectories could be tracked under the time-varying external interface and unknown internal uncertainties. These five ships start from different starting points and can finally maintain a certain formation scheme through continuous control as shown in Circle 1, 2, 3, 4, and 5. The posture control performance and formation performance can be observed by the comparison between the curve part and straight section referred to in Figs. 13 and 14. The kinetics errors of the surge, sway, and yaw motion speed are guaranteed within a small neighborhood of zero as shown in Fig. 14. y_e and η_e are proven to be stable as shown in Fig. 13, which shows that x_e is stable as well. By using RBFNNs and adaptive estimation law, the uncertain dynamics and unknown disturbances are well approximated and estimated in Figs. 15 and 16.

Remark 5.3. Compared to Route 1, the kinetics errors perform well due to the concentration on virtual speed controller design. However, the kinematics errors fluctuate a little violently, we think this is caused by the drastic change in the desired trajectory and formation structure. Compare with Route 1, due to a large number of curves, Route 2 amplifies the kinematic and kinetic errors caused by the formation structure itself. The speeds and accelerations between leader and followers begin to increase, while the proposed controller certainly has some control effects on complex routes.

6. Conclusion

In this research, to extend the application scope of the ship formation controller, the characteristics of heterogeneous ships are summarized. Based on that, isomorphic and heterogeneous ships are selected to verify the effectiveness of the proposed controller. Besides the heterogeneous features, the problems of unknown disturbance and unknown dynamics are solved by the proposed formation controller. Both the ship kinematics control and kinetics control are proven to be uniformly bounded through the stability analysis, and the results verify the effectiveness of the theory. The proposed formation structure is capable of switching the formation problem into a trajectory tracking problem, which may contribute to the actual formation application of large cargo ships. Also, the formation results on isomorphic and heterogeneous ships demonstrate the adaptability and effectiveness of the proposed controller on general ships.

For future work, the formation error analysis on formation structure and routes need to be further investigated. Besides that, the consideration of heterogeneous formation needs to be studied on dynamic differences mentioned in Section 1, which can be considered by using extended state observer (ESO) with sliding mode control method due to its advantage on unknown ship dynamics and disturbances. However, it can only solve the problem partly because of the dynamic changes in ship parameters. Moreover, ship collision avoidance problems need to be further handled before the formation becomes steady. Also, reinforcement learning and other advanced technologies are attractive to put into use for real ship formation applications.

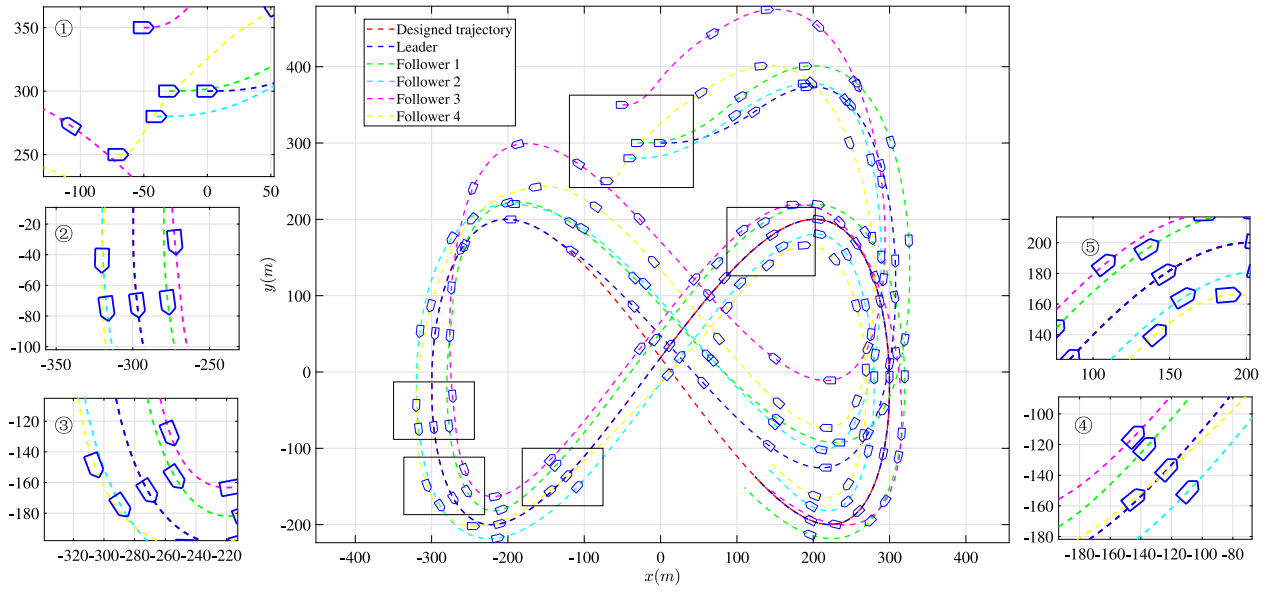

Fig. 12. The performance of the tracking and formation control in Route 2.

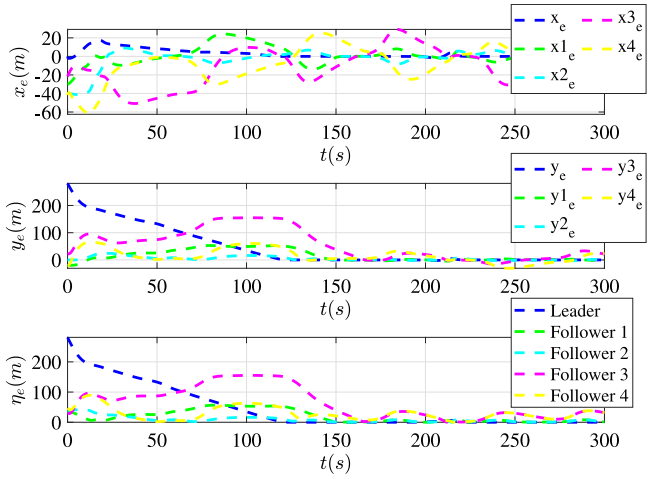

Fig. 13. The kinematics errors of the follower and leadership for heterogeneous formation in Route 2.

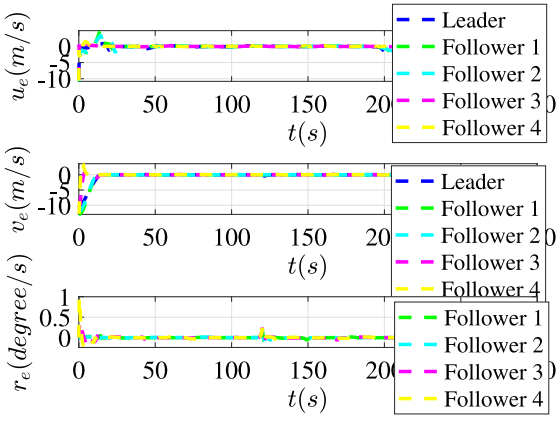

Fig. 14. The kinetics errors of the follower and leadership for heterogeneous formation in Route 2.

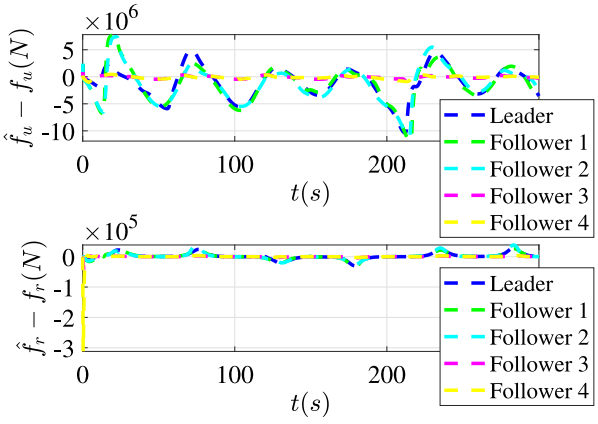

Fig. 15. The approximation values of the ship uncertain dynamics between leader and followers for heterogeneous formation in Route 2.

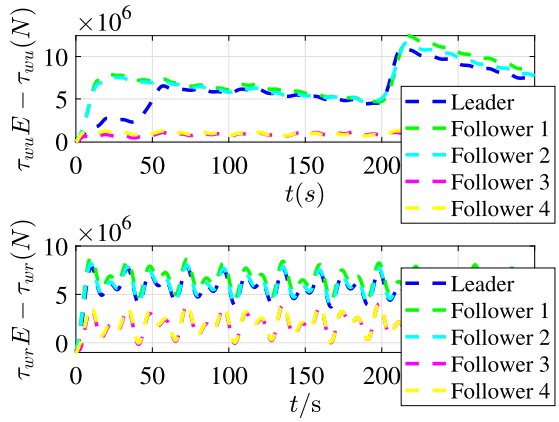

Fig. 16. The estimation of the upper bound on external disturbances on heterogeneous formation in Route 2.

CRediT authorship contribution statement

Xu You: Conceptualization of this study, Methodology, Software, Writing – original draft. **Xinping Yan:** Writing – review & editing, Supervision, Funding acquisition. **Jialun Liu:** Writing – review & editing, Supervision. **Shijie Li:** Writing – review & editing, Supervision. **Rudy R. Negenborn:** Writing – review & editing.

Declaration of competing interest

The authors declare that they have no known competing financial interests or personal relationships that could have appeared to influence the work reported in this paper.

Data availability

The authors do not have permission to share data.

References

Arrichiello, F., Chiaverini, S., Fossen, T.I., 2006. Formation control of underactuated surface vessels using the null-space-based behavioral control. In: IEEE International Conference on Intelligent Robots and Systems. IEEE, pp. 5942–5947.

Bhat, S.P., Bernstein, D.S., 2000. Finite-time stability of continuous autonomous systems. SIAM J. Control Optim. 38 (3), 751–766.

Breivik, M., Hovstein, V.E., Fossen, T.I., 2008. Ship formation control: A guided leader-follower approach. IFAC Proc. Vol. (IFAC-PapersOnline) 17 (1 PART 1), 16008–16014.

Chen, L., Huang, Y., Zheng, H., Hopman, H., Negenborn, R., 2019. Cooperative multi-vessel systems in urban waterway networks. IEEE Trans. Intell. Transp. Syst. 21 (8), 3294–3307.

Chen, H., Peng, Y., Wang, Y., Xie, S., Yan, H., 2020. Leader–follower close formation control for underactuated surface vessel via terminal hierarchical sliding mode. Int. J. Adv. Robot. Syst. 17 (3), 1729881420921012.

Chen, Y.Q., Wang, Z., 2005. Formation control: a review and a new consideration. In: 2005 IEEE/RSJ International Conference on Intelligent Robots and Systems. IEEE, pp. 3181–3186.

Colling, A.P., Hekkenberg, R.G., 2019. A multi-scenario simulation transport model to assess the economics of semi-autonomous platooning concepts. In: Proceedings of the International Conference on Computer Applications and Information Technology in the Maritime Industries (COMPIT), Tullamore, Ireland, Vol. 25. pp. 132–145.

Colling, A., Hekkenberg, R., van Hassel, E., 2021. A viability study of waterborne platooning on the lower Rhine. Eur. J. Transp. Infrastruct. Res. 21 (2), 71–94.

Das, B., Subudhi, B., Pati, B.B., 2016. Cooperative formation control of autonomous underwater vehicles: An overview. Int. J. Autom. Comput. 13 (3), 199–225.

Do, K.D., Jiang, Z.-P., Pan, J., 2004. Robust adaptive path following of underactuated ships. Automatica 40 (6), 929–944.

Fossen, T.I., 2011. Handbook of Marine Craft Hydrodynamics and Motion Control. John Wiley and Sons.

Fu, M.Y., Yu, L.L., Jiao, J.F., Xu, Y.J., 2017. Formation control of autonomous surface vessels with saturation constraint. Kongzhi Lilun Yu Yingyong/Control Theory Appl 34 (5), 663–670.

Gao, Z., 2006. Scaling and bandwidth-parameterization based controller tuning. In: Proceedings of the American Control Conference, Vol. 6. pp. 4989–4996.

Ghommem, J., Mnif, F., Poisson, G., Derbel, N., 2007. Nonlinear formation control of a group of underactuated ships. In: OCEANS 2007 - Europe, Vol. 41. IEEE, pp. 1–8.

Gu, N., Wang, D., Peng, Z., Liu, L., 2019. Distributed containment maneuvering of uncertain under-actuated unmanned surface vehicles guided by multiple virtual leaders with a formation. Ocean Eng. 187 (October 2018), 105996.

Haseltalab, A., Chen, L., Colling, A., Borst, L., Garofano, V., Hekkenberg, R., Negenborn, R.R., 2019. Waterborne platooning by smart vessels for smart shipping. Naval Archit..

Jin, X., Dai, S.-L., Liang, J., Guo, D., 2021. Multirobot system formation control with multiple performance and feasibility constraints. IEEE Trans. Control Syst. Technol..

Li, Y., Zheng, J., 2018. The design of ship formation based on a novel disturbance rejection control. Int. J. Control Autom. Syst. 16 (4), 1833–1839.

Liu, H., Peng, F., Modares, H., Kiumarsi, B., 2021. Heterogeneous formation control of multiple rotorcrafts with unknown dynamics by reinforcement learning. Inform. Sci. 558, 194–207.

Liu, L., Wang, D., Peng, Z., Li, T., 2017. Modular adaptive control for LOS-based cooperative path maneuvering of multiple underactuated autonomous surface vehicles. IEEE Trans. Syst. Man Cybern. Syst. 47 (7), 1613–1624.

Lu, Y., Zhang, G., Sun, Z., Zhang, W., 2018. Robust adaptive formation control of underactuated autonomous surface vessels based on MLP and DOB. Nonlinear Dynam. 94 (1), 503–519.

Meersman, H., Moschouli, E., NanwayBoukani, L., Sys, C., van Hassel, E., Vanelslander, T., Van de Voorde, E., 2020a. Evaluating the performance of the vessel train concept. Eur. Transp. Res. Rev. 12 (1), 1–11.

Meersman, H., Moschouli, E., Sys, C., Van de Voorde, E., Vanelslander, T., van Hassel, E., Friedhoff, B., Hoyer, K., Tenzer, M., Hekkenberg, R., 2020b. Identifying cost performance indicators for a logistics model for vessel trains. In: Maritime Supply Chains. Elsevier, pp. 47–65.

Munim, Z.H., 2019. Autonomous ships: a review, innovative applications and future maritime business models. In: Supply Chain Forum: An International Journal. 20, (4), Taylor & Francis, pp. 266–279.

Novimar, 2017. Novimar researches a new system of waterborne transport operations. [EB/OL]. https://novimar.eu/ Accessed July 12, 2017.

Oh, K.-K., Park, M.-C., Ahn, H.-S., 2015. A survey of multi-agent formation control. Automatica 53, 424–440.

Peng, Z., Wang, J., Wang, D., Han, Q.-L., 2020. An overview of recent advances in coordinated control of multiple autonomous surface vehicles. IEEE Trans. Ind. Inf. 3203 (c), 1.

Polyakov, A., 2011. Nonlinear feedback design for fixed-time stabilization of linear control systems. IEEE Trans. Automat. Control 57 (8), 2106–2110.

Polycarpou, M.M., 2001. Fault accommodation of a class of multivariable nonlinear dynamical systems using a learning approach. IEEE Trans. Automat. Control 46 (5), 736–742.

Rahimi, R., Abdollahi, F., Naqshi, K., 2014. Time-varying formation control of a collaborative heterogeneous multi agent system. Robot. Auton. Syst. 62 (12), 1799–1805.

Ren, W., Cao, Y., 2011. Distributed Coordination of Multi-Agent Networks: Emergent Problems, Models, and Issues, Vol. 1. Springer.

Riahifard, A., Rostami, S.M.H., Wang, J., Kim, H.J., 2020. Adaptive leader-follower formation control of under-actuated surface vessels with model uncertainties and input constraints. Appl. Sci. (Switzerland) 10 (7).

Shen, Z., 2019. Adaptive Sliding Mode Control for Trajectory Tracking of Underactuated Ships. Science Press, Beijing.

Shimin, W., Zhi, Z., Zhong, R., Yuanqing, W., Zhouhua, P., 2020. Adaptive distributed observer design for containment control of heterogeneous discrete-time swarm systems. Chin. J. Aeronaut. 33 (11), 2898–2906.

Sun, Z., Zhang, G., Lu, Y., Zhang, W., 2018. Leader-follower formation control of underactuated surface vehicles based on sliding mode control and parameter estimation. ISA Trans. 72 (December), 15–24.

Wang, N., Li, H., 2020. Leader–follower formation control of surface vehicles: A fixed-time control approach. ISA Trans..

Wang, J., Wang, C., Wei, Y., Zhang, C., 2020a. Filter-backstepping based neural adaptive formation control of leader-following multiple AUVs in three dimensional space. Ocean Eng. 201 (February), 107150.

Wang, J., Wang, C., Wei, Y., Zhang, C., 2020b. Sliding mode based neural adaptive formation control of underactuated AUVs with leader-follower strategy. Appl. Ocean Res. 94 (July 2019), 101971.

Yuan, C., Licht, S., He, H., 2017. Formation learning control of multiple autonomous underwater vehicles with heterogeneous nonlinear uncertain dynamics. IEEE Trans. Cybern. 48 (10), 2920–2934.

Zereik, E., Bibuli, M., Mišković, N., Ridao, P., Pascoal, A., 2018. Challenges and future trends in marine robotics. Annu. Rev. Control 46, 350–368.

Zheng, Y., Zhu, Y., Wang, L., 2011. Consensus of heterogeneous multi-agent systems. IET Control Theory Appl. 5 (16), 1881–1888.